

Cardiovascular Magnetic Resonance Imaging

Textbook and Atlas

Bearbeitet von
Vinzenz Hombach, Nico Merkle, Volker Rasche

1., Auflage 2012 2012. Buch. 512 S. Hardcover
ISBN 978 3 7945 2799 1
Format (B x L): 21 x 28 cm
Gewicht: 1928 g

[Weitere Fachgebiete > Medizin > Klinische und Innere Medizin > Kardiologie,
Angiologie, Phlebologie](#)

Zu [Inhaltsverzeichnis](#)

schnell und portofrei erhältlich bei


DIE FACHBUCHHANDLUNG

Die Online-Fachbuchhandlung beck-shop.de ist spezialisiert auf Fachbücher, insbesondere Recht, Steuern und Wirtschaft. Im Sortiment finden Sie alle Medien (Bücher, Zeitschriften, CDs, eBooks, etc.) aller Verlage. Ergänzt wird das Programm durch Services wie Neuerscheinungsdienst oder Zusammenstellungen von Büchern zu Sonderpreisen. Der Shop führt mehr als 8 Millionen Produkte.

26.5 CT of Cardiac Structure and Function

CT imaging has a relatively high spatial resolution, and a high contrast between the blood pool and other tissues can be achieved after the injection of an iodinated contrast agent. CT has the ability to provide high-resolution morphologic imaging of the heart and adjacent thoracic vessels (Figure 26-10). With a contrast administration regimen including a dense bolus for the left cardiac structures followed by a saline flush supplemented with a low fraction of contrast agent, both the left and right sided cardiac cavities can be well discerned against the myocardium and the epicardial fat pad (Figure 26-1). Clinically, however, CT imaging does not play a very prominent role for this indication. Both echocardiography and magnetic resonance imaging (MRI) can provide all relevant information in most clinical situations.

Quantitative analysis of cardiac chamber geometry and ventricular function is an essential part of a complete cardiac evaluation. MRI is currently considered the standard of reference for ventricular global and regional function analysis. As part of a retrospectively gated cardiac imaging study CT can provide an anatomically precise evaluation of chamber morphology and function, along with a detailed assessment of coronary and valvular anatomy. Global LV functional parameters calculated from CT datasets acquired

utilizing > 64 detector technology correlate well with MRI in daily clinical practice (van der Vleuten 2009). They may be considered interchangeable. However, MRI datasets are acquired without any ionizing radiation dose and no need to administer contrast agents. Functional CT data are only available utilizing high dose retrospective helical ECG-gating or continuous acquisition of a full cardiac cycle utilizing a 16 cm detector. Modern dose saving technology allows morphologic coronary and cardiac imaging at a dose exposure of 1–4 mSv. Both high-pitch helical scanning and prospectively gated coronary CT angiography restrict dose exposure to one quiescent cardiac phase without acquisition of the full cardiac cycle in order to achieve substantial dose reductions. Functional cardiac analysis is not permitted by these technologies. In other words, CT functional data require a dose exposure in the range of 10–20 mSv almost 10 times the dose we acquire from natural sources during a full year. Such a high dose exposure is not warranted for the purpose of functional and morphologic cardiac analysis, which can be achieved with other modalities at the same level of accuracy. But contraindications for MRI preclude imaging in patients with the majority of pacemakers, intracardiac defibrillators (ICD) or cardiac resynchronization systems (CRT). MDCT derived functional analysis constitutes a viable alternative for this subset of patients. One restriction though applies for CT functional imaging, the flow sensitivity that is clinically very useful for both echocardiography and MRI cannot be achieved with CT imaging.

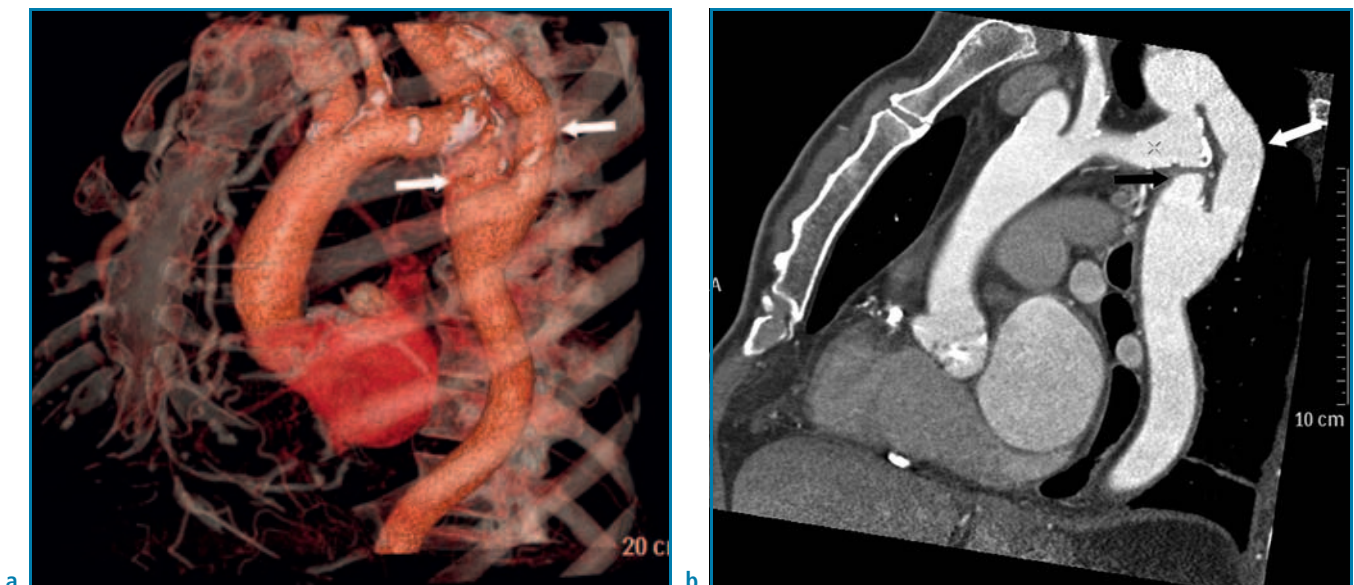


Figure 26-10 Thoracic morphology scans show congenital coarctation with a complete occlusion of the native aorta (small arrows in (a), (b)). The coarctation was surgically treated with an extra-anatomical bypass (large arrows in (a), (b)).

26.6 Myocardial Perfusion and Viability

Myocardial perfusion is one of the most important prognostic indicators for patient outcome in the management of CAD. The comprehensive assessment of myocardial perfusion and morphologic coronary artery evaluation has been shown to provide incremental diagnostic value over either technique alone (van Werkhoven 2009). So far image fusion of two modalities (e.g. nuclear perfusion testing and coronary CT angiography) was necessary to provide the comprehensive morphology and function assessment. CT, though, has the potential to achieve the coveted goal of a stand-alone modality providing both morphology and function of a stenotic lesion. At the time of this writing no vigorous clinical trials testing the diagnostic accuracy of CT-based perfusion scanning have been completed, but first feasibility trials indicate the potential of both snapshot CT perfusion (Figure 26-11) and first-pass imaging with rapid successive frame acquisition (George 2009). Initial dose exposure calculations for the additional CT perfusion scanning render values in the range of 5–10 mSv, which compares very favorably to

nuclear stress testing but very unfavorably to the 0 mSv of MRI perfusion imaging. Clinical trials are ongoing to establish the best perfusion imaging modality to be combined with CT coronary angiography.

The determination of myocardial viability is playing an increasing role in predicting the success of revascularization therapy. Delayed contrast-enhanced imaging with MR detects accumulation of gadolinium-based chelates in areas of myocardial necrosis after infarction. The same principles may apply to cardiac CT, since iodine-based intravenous contrast material has similar kinetics as gadolinium chelates. Low kilovoltage (e.g. 80 kVp) protocols have been shown to result in better iodine contrast differentiation and the additional radiation dose exposure for performing viability imaging with CT was quantified at 3.8 mSv in females and 2.8 mSv in males. But the contrast sensitivity of MRI easily outperforms CT imaging for the purpose of viability testing, this was validated in trials showing a systematic underestimation of the true infarct size by CT compared with MRI (Nieman 2008). MR imaging with superior gadolinium contrast sensitivity is therefore considered the standard of reference for this application.

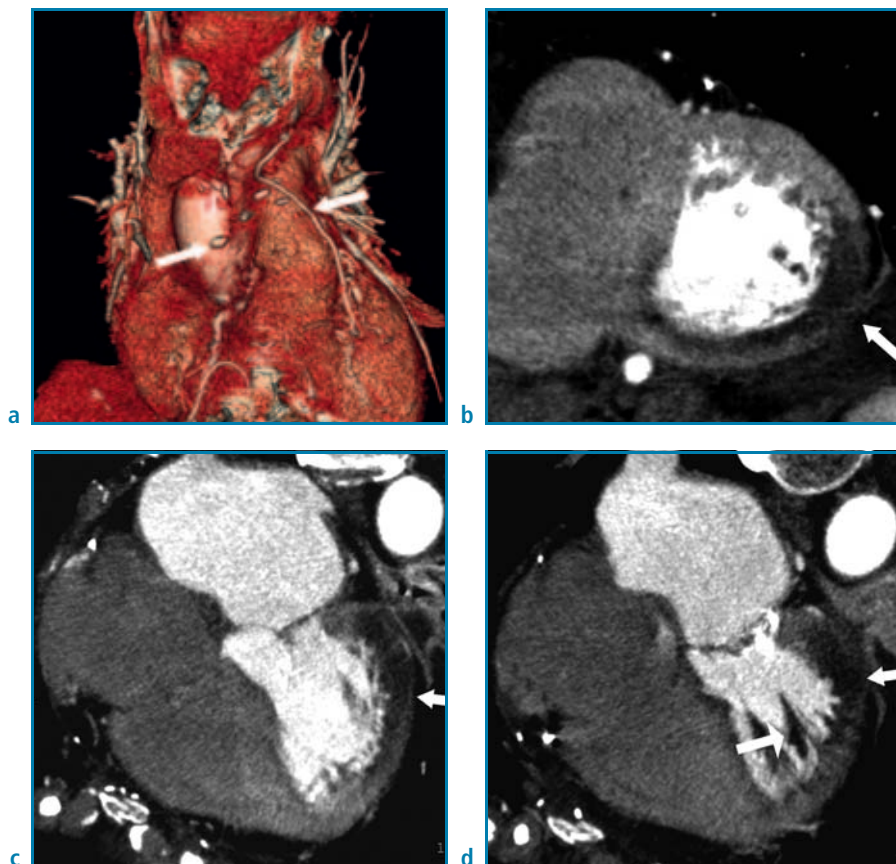


Figure 26-11 Patients presents 6 d post-surgery with suspected graft occlusion. A high-grade left main stenosis with acute lumen occlusion initiated the aortocoronary bypass grafting. The mammary pedicle (thick arrow) to the LAD is patent, but the venous graft to the LCX (thin arrow in (a)) is occluded. This induced acute ischemia in the LCX territory as apparent on the early enhancing snapshot images oriented along short-axis planes (b) and long-axis planes in mid-ventricular position (c) and papillary muscle coverage (d). The large hypodense perfusion defect in the lateral wall (arrows in (b–d)) also affects the papillary muscular structures (thin arrow in (d)).

26.7 Pericardial Disease

The pericardium is usually embedded in epi- and pericardial fat that separates the pericardial layers from the myocardium. CT imaging shows a very low density or attenuation of fat (0 to ~ 100 HU) which is easily contrasted against both myocardium and pericardium (both ~ 50 HU). This allows to discern a thin line of normal thickness pericardium (range between 1–2 mm) against the myocardium if the epicardial fat layer is thin enough. It usually appears as a thin line and is best delineated on the anterior surface of the heart (Breen 2001).

Visualization of the pericardium is relevant for various congenital and acquired conditions. Congenital absence of the pericardium can be complete or partial. The condition is infrequent, and patients are usually asymptomatic. A CT scan can be helpful in establishing the absence or presence of a segment of pericardium, but lack of visualization of the pericardium, especially on the posterior surface, is not a sufficient criterion for making the diagnosis.

The normal pericardial thickness is 1–2 mm on high resolution CT scans, pericardial thickening of more than 4–6 mm, even if only localized can be helpful in suspected constriction. Thickened pericardium can be found in many situations, including the early post-operative period, uremia, rheumatic heart disease, and sarcoidosis or as a consequence of radiation therapy. It does not constitute proof of constriction per se. Constrictive pericarditis is associated with calcifications in the late to chronic course of the disease, CT

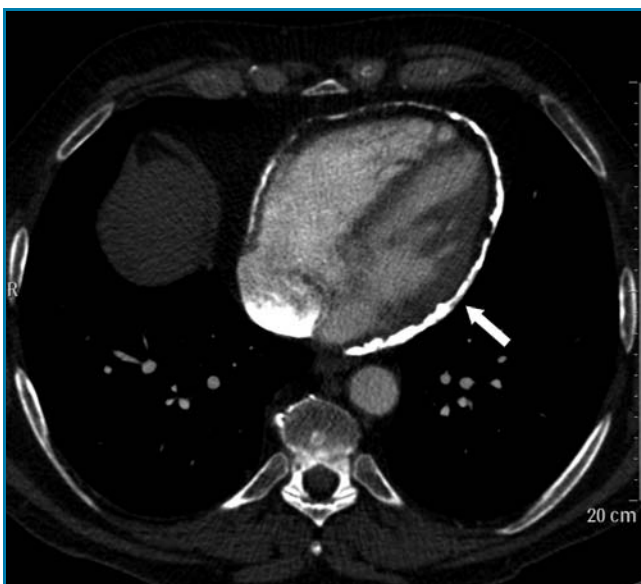


Figure 26-12 Constrictive pericarditis: A non-gated thoraco-abdominal CT acquired for non-cardiac purposes shows the calcified pericardium (arrow) surrounding the ventricles and part of the atria.

imaging is very well-suited to delineate the calcified pericardium even without contrast administration (Figure 26-12).

Pericardial fluid can be reliably detected on CT images. Though echocardiography is the first line modality for this purpose, CT imaging may be supplemental in cases of limited acoustic windows. Other findings easily discerned on high resolution CT images are pericardial, bronchogenic cysts or teratomas. Primary neoplasms of the pericardium are infrequent but can be the reason for thickened pericardium on CT scans. The density of a pericardial effusion can be indicative of its origin, a serous fluid effusion would be close to the density of water (0–20 HU) while a bloody pericardial effusion would be measured around 50 HU.

26.8 Diagnosis of Cardiac Masses

Echocardiography is the first line modality for the detection of cardiac masses. But both MRI and CT may supplement the echo findings with additional information because of their ability to visualize cardiac morphology without the restriction of acoustic windows. MRI is superior in its ability to provide tissue characterization and differentiation. CT is only superior in its sensitivity for calcified structures and high spatial resolution undisturbed by flow artifacts. CT density or attenuation measurements (Hounsfield [HU] values) do provide some limited insight into the tissue nature of a mass. Lipomas appear with very low HU values (around 0 HU), whereas cysts have water-like attenuation values (0–10 HU). CT numbers of intracardiac thrombi usually range from 20–90 HU and show substantial overlap with myocardial structures (around 50 HU). CT is very sensitive to identify thrombi in the left atrial appendage but has limited specificity with a large number of false positives generated by slow contrast inflow in patients with atrial fibrillation or flutter (Hur 2009). The most frequent cardiac tumor, atrial myxoma, is represented by a chamber filling defect on cardiac CT images (Figure 26-13).

26.9 CT Imaging for Left Atrial Electrophysiology Applications

Cardiac CT angiography can assess atrial anatomy, pulmonary venous anatomy and coronary venous anatomy, all with great relevance to left atrial arrhythmias including atrial fibrillation, atypical atrial flutter circuits and focal atrial tachycardia. Catheter-based techniques for ablation of



Figure 26-13 Left atrial myxoma becomes apparent on CT images (a) as a filling defect (round structure in the left atrium marked with an arrow). Smaller lesions with thrombotic and lipidic components may be easily missed on axial images but are readily apparent on cardiac long-axis views (b) (doubling of atrial septum, arrow in (b)).

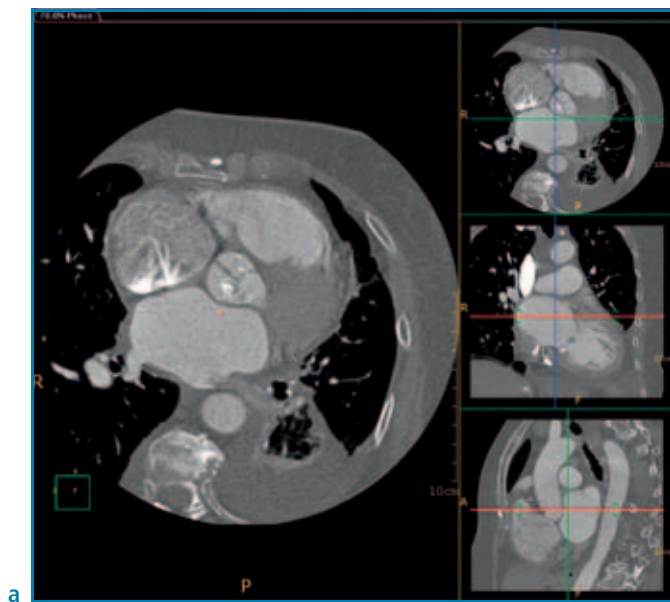
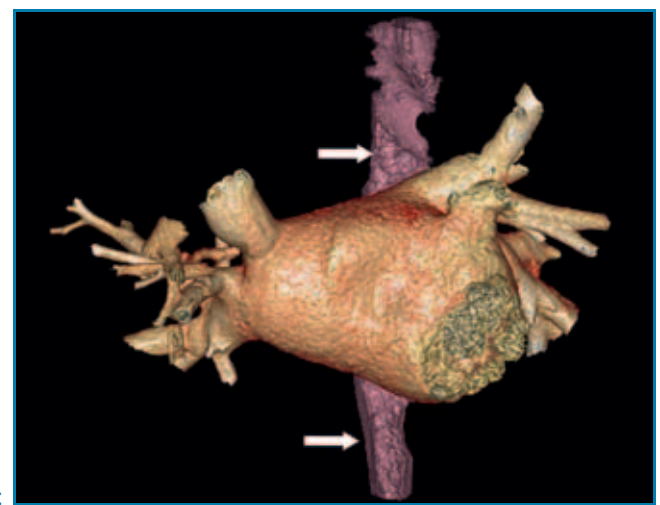
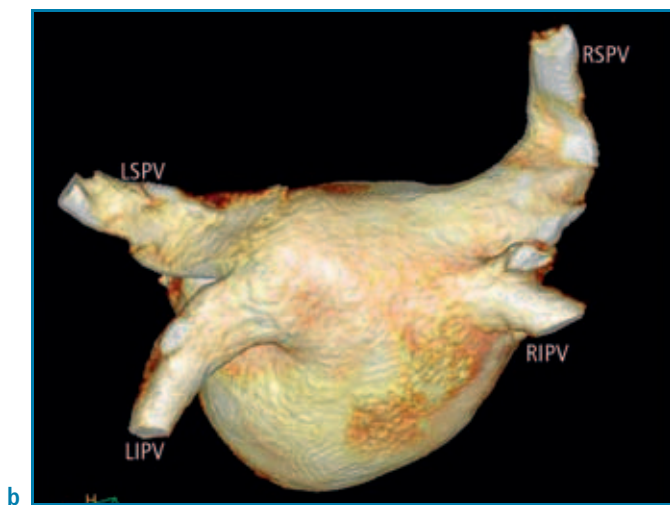


Figure 26-14 Cross-sectional CT images (a) in transverse (tra), coronal (cor) and sagittal (sag) orientation with the left atrium (LA) in the imaging center. The left atrium is extracted from the cross-sectional dataset and displayed in three-dimensional shape (b). The case sample has four pulmonary vein ostia with the right superior pulmonary vein (RSPV), the right inferior pulmonary vein (RIPV), the left superior pulmonary vein (LSPV) and the left inferior pulmonary vein (LIPV) marked in the volume rendering. The esophagus (purple structure marked with arrows) is in close proximity to the posterior wall of the left atrium (c).



atrial fibrillation have focused on ablation of the pulmonary veins with either segmental ablation or complete circumferential electrical isolation of the pulmonary veins. CT imaging can characterize these features through three-dimensional volume rendered and endocardial or endoscopic images (Figure 26-14). The number of veins, the location in the atrium, the vein size and the vein morphology including ostial complexity are easily shown (Blanke 2010). Pre-interventional CT angiography can provide a roadmap of atrial and pulmonary vein structure to guide electrophysiology studies and ablation of atrial fibrillation. The integration of 3D CT images obtained before the procedure (Figure 26-14b) may be realized in a navigation system for real-time catheter positioning (Bertaglia 2009). In addition to the anatomic image generation for intraprocedural orientation, CT imaging of the atrial appendage has been shown to detect thrombus filling defects with a very high sensitivity compared to transesophageal echocardiography.

Pulmonary vein stenosis is a potential complication of atrial fibrillation ablation. CT and MRI have been used to diagnose pulmonary vein stenosis. Pre-operative studies, in addition to providing a roadmap for intervention, can provide a template for follow-up studies assessing the time course of pulmonary venous remodeling and stenosis formation after ostial ablation.

The 3D relationship of the left atrium and the esophagus may have relevance to atrial fibrillation ablation approaches,

as left atrial-esophageal fistula have been reported as a fatal complication. There is variability in the course of the esophagus and degree of contact between the posterior left atrial wall and the anterior circumference of the esophagus. This can be visualized by CT imaging (Figure 26-14c).

26.10 Angiography of the Thoracic and Abdominal Aorta

Aortic aneurysms are associated with risk for sudden death due to aortic dissection or rupture. The disease may be induced by connective tissue disorders or acquired cardiovascular atherosclerosis. CT angiography can diagnose aortic aneurysms (Figure 26-15), dissection (Figure 26-16), and wall abnormalities such as penetrating ulcers, intramural hematoma and atherosclerotic plaque rupture in all segments. CT-based angiography of the aorta has emerged as the preferable imaging modality for all aortic emergencies. Whereas recent generations of CT technology were still suffering from pulsation artifacts in the ascending aorta mimicking dissection membranes, this does no longer apply to today's editions with more than 64 detector rows. Accurate delineation of dissection membranes outperforms invasive angiography to visualize the intimal tear and re-entry



Figure 26-15 CT imaging of the full length of the aorta (a) shows a lumen dilatation of the infrarenal abdominal aorta (arrow). The infrarenal aneurysm shows partial lumen thrombosis as demonstrated in the sagittal section (arrow) (b).

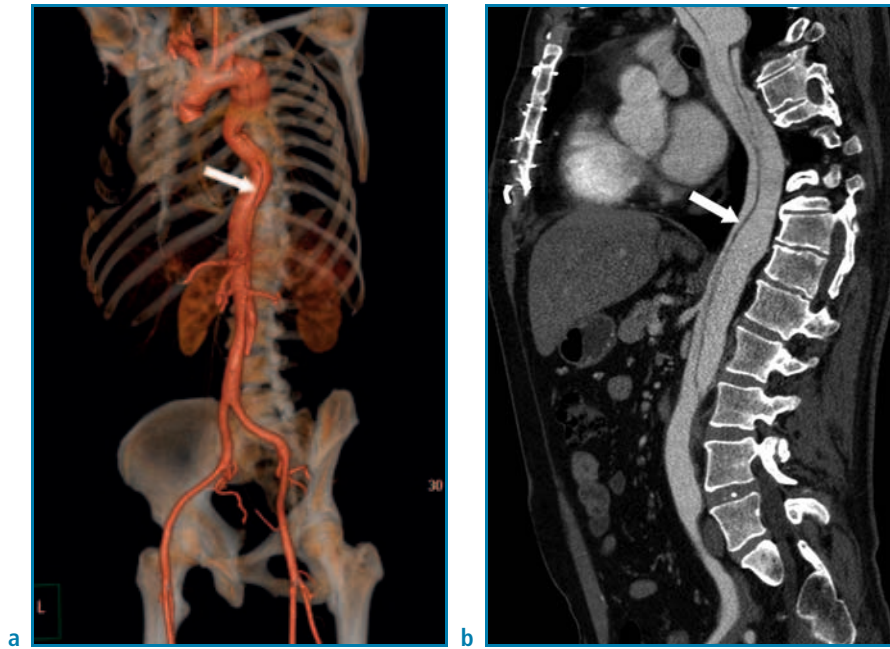


Figure 26-16 A dissection, affecting the descending aorta is visualized on both volume rendering (a) and sagittal cross-section (b). The dissection is related to an aneurysm formation in the proximal descending aorta. The arrows in (a) and (b) mark the dissection membrane extending in full length from the proximal to the distal part of the descending aorta.



Figure 26-17 Patient with acute traumatic rupture of the proximal descending aorta. The lesion was repaired with endovascular grafting. The endovascular stent graft (arrow) is well visualized both with and without anatomical overlay by CT volume rendering images.

lesions (Figure 26-16). CT imaging is considered the gold standard for the detection of endoleaks after endo-graft occlusion of aneurysm formations. Young patients should be carefully selected for elective CT imaging due to high dose exposure rates associated with the procedure, MRA may be a good alternative in stable or chronic situations. Recent scanner generations have substantially alleviated the problem with dramatic dose reductions realized. As of today the lowest dose for imaging of the thoracic aorta is realized by so-called prospectively ECG-gated image acquisition techniques (Sommer 2010). This phenomenon founds the basis for the combination of pulmonary arterial, thoracic aortic and coronary angiographic imaging in a single ECG-gated chest CT scan, the so-called triple-rule-out protocol. CT imaging of the aorta allows accurate visualization of endovascular stent grafts (Figure 26-17).

26.11 Role of CT for Transcatheter Aortic Valve Implantation (TAVI)

Transcatheter aortic valve implantations have emerged in the last years as an alternative treatment for aortic stenosis. Two first generation devices are available for human implantations today (Grube 2007, Cribier 2009). The native stenotic valve is initially dilated with a valvuloplasty balloon under rapid pacing. Subsequently a bioprosthesis composed of either porcine or bovine pericardium is implanted into

the native annular orifice. The bioprosthesis is mounted on a stent frame which serves two purposes: it unfolds the new valve into functional position and pushes the native valve aside into the sinus of Valsalva pouches. The Edwards Sapien valve is balloon mounted and able to cover aortic root sizes up to 26 mm diameter. The device is well-suited for a transapical deployment via a 5 cm left intercostal incision. The Core Valve device is self-expanding and the method of choice for a percutaneous purely catheter-based approach. It will cover aortic annulus sizes up to 27 mm. The method is considered an alternative treatment for non-surgical candidates only. We can very well predict the durability of surgically implanted devices today but long-term survival and durability data for the transcatheter devices are missing. It will therefore take many more years until the question will be answered: How many surgical candidates can be safely converted for transcatheter approaches?

The critical questions asked during the planning of transcatheter procedures today relate to the size and morphology of the aortic root and the access pathway (transfemoral or transsubclavian or transapical). All these questions pertinent to transcatheter aortic valve replacements can be safely addressed with a supplemental set of diagnostic imaging modalities only. Transthoracic echocardiography is the first line of testing for appropriate annular size and grading of severity of aortic valve stenosis. Invasive angiography is still needed in the majority of cases to rule out or percutaneously treat coronary artery disease. CT coronary angiography would not be appropriate as we are dealing with high pre-test probability populations with a very high propensity for calcifications. But CT is well-suited with its very high sensitivity for calcifications to delineate the distribution of calcium in the aortic root and valvular leaflets. This is the reason why most clinicians today endorse a multi-modality strategy for the assessment of potential TAVI candidates encompassed of echocardiography, invasive coronary angiography and CT angiography for aortic root assessment and peripheral vascular access evaluation.

Multi-slice computed tomography may be the most comprehensive non-invasive imaging modality to evaluate potential candidates for transcatheter aortic valve replacement. This three-dimensional imaging technique provides accurate information on anatomical aspects of the aortic valve, aortic root and surrounding structures (such as the coronary arteries), aorta and peripheral arteries (Figure 26-18). The high accuracy of this technique to measure the aortic valve opening area by planimetry of the stenotic orifice has been shown. Furthermore, with the use of multi-phase data sets obtained during ECG gating, motion of the cusps can be evaluated. At the current stage of development the concern of radiation dose exposure associated with the retrospective helical acquisition does not apply in this

setting. Most of the patients included for TAVI assessment are octogenarians with little chance to survive long enough for the initiation of radiation induced cancer.

The main application of MDCT imaging is to visualize and quantitatively assess the aortic root. MDCT has a major advantage over MR in this respect. Within a few seconds a complete 4D dataset can be acquired with calcium sensitivity to the benefit of TAVI assessment. The most important lesson learned from a regular application of CT so far concerns the aortic annulus (Schultz 2010). So far a singular diameter was measured mostly utilizing transthoracic echocardiography (TTE). The heart is viewed in the left long parasternal axis and the aortic annulus is measured at the caudal insertion of the valve leaflets. CT measurements were initially carried out in similar fashion measuring a singular diameter in the coronal plane. It was found that the CT derived annular diameters though very accurately calibrated were significantly larger compared to TTE diameters. In order to clarify this discrepancy two-dimensional diameter measurement carried out on a cross-sectional plane were carried out on CT images. The cross-sectional plane corresponding to the aortic annulus was defined by three points. Each point was defined by the three nadirs of the aortic cusp insertion line into the aortic root. It was found that most of the annulus formations were not circular but elliptical. This resulted in a systematic overestimation of aortic annular dimensions in the coronal (used in CT) vs. the sagittal (used in echocardiography) imaging plane. Today's consensus in the TAVI community therefore recommends not to use maximum or singular plane diameters any more. Precise TAVI device planning should rely on either cross-sectional area measurements directly or be based on mean values derived from the maximum and minimum diameters of the annular ellipse (Figure 26-18). The annular diameter may be used for both balloon selection for valvuloplasty and device sizing for the revalving procedure. ECG-gated MDCT will most likely emerge as the standard of reference for acquiring these measurements.

Additional information obtained from the cardiac and vascular CT scan includes individual C-arm angulations and access planning (Figure 26-18). The CT scan reconstructed in a quiescent cardiac phase (either end-systole or mid-diastole) will show the aortic root including the valvular leaflets. In order to position the transcatheter device correctly it is essential to find a fluoroscopy plane perpendicular to the aortic root with all three leaflet structures projected in-line. Other measurements with importance for TAVI planning that can be easily obtained from CT scans are distance of the coronary ostia to the annular plane, width of the sinotubular junction, diameter of the proximal ascending aorta, and extent of calcification present on the leaflet structures.

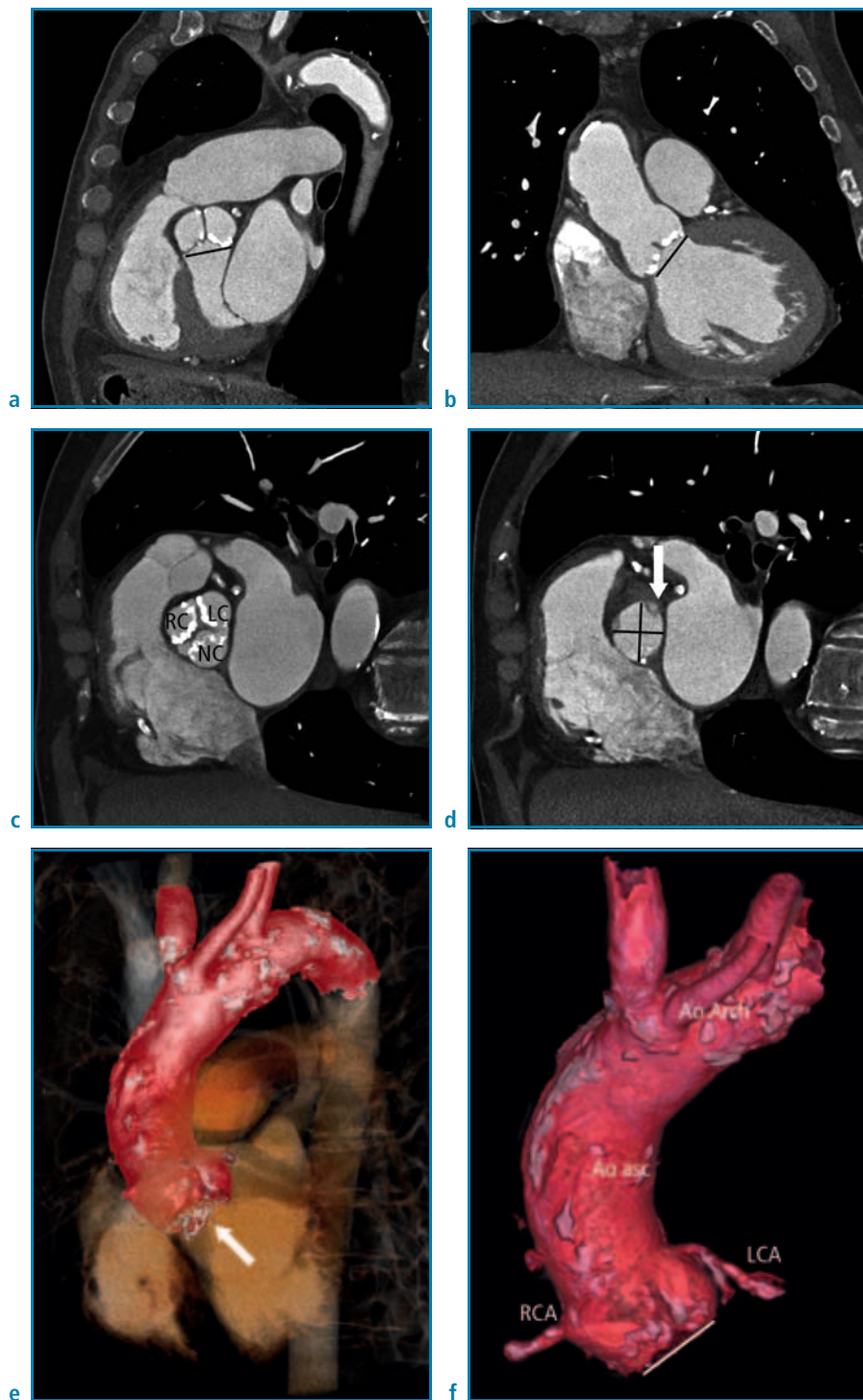


Figure 26-18 Sagittal (a) and coronal (b) sections at the level of the aortic root demonstrate an aortic valve with calcified leaflets. The aortic annulus is measured in a double oblique plane oriented along the basal attachments of the leaflets (black line in (a) and (b)). Double oblique plane (c) shows calcifications of the free edges. Double oblique plane (d) oriented along the black line of (a) and (b). The basal attachments are visualized as small circular structures (arrow). The annulus is typically elliptical and not circular. The mean value of the largest and smallest diameter is used for sizing the appropriate endovascular device (black lines forming a cross). Volume rendering (e) in anteroposterior projection shows the calcified valvular structures at the base of the ascending aorta (arrow). The 3D volume rendering of the isolated aortic root (f) can be used to determine the C-arm position for TAVI implantation procedures. In this case the root is rotated in an LAO projection with a cranial tilt. This allows perpendicular viewing of the annulus with all sinuses projection along a singular plane (line in (f)). Ao Arch: aortic arch; Ao asc: ascending aorta; LC: left coronary sinus; LCA: left coronary artery; NC: non-coronary sinus; RC: right coronary sinus; RCA: right coronary artery.

The feasibility of a transfemoral approach depends strongly on the size, calcification and tortuosity of the iliofemoral arteries and aorta. Current devices require 18 French introducer sheaths and cross-sectional diameters of < 6 mm would contraindicate a transfemoral approach. Bulky calcifications and angulations of the thoracic aorta may also render

a transapical approach the procedure of choice to minimize the risk of vascular complications. Regardless of the vascular access, severe aortic dilatation at the level of the sinotubular junction (> 45 mm) is considered a contraindication for self-expandable stent frames.

26.12 Detection of Pulmonary Embolism

Acute pulmonary embolism (PE) is a potentially life-threatening complication of peripheral deep venous thrombosis (DVT). A certain number of patients with massive pulmonary embolism do not receive any imaging tests because they either die before the diagnosis is suspected or are hemodynamically unstable precluding any transportation for the imaging procedure. In other words patients who are referred for imaging have to be in a sufficiently stable clinical condition. The role of imaging is to confirm or rule out the diagnosis of acute PE; and, if possible, to establish an alternative diagnosis. This is important because 60% of patients have a false positive clinical suspicion of PE. CT angiography is presently the workhorse for the evaluation of stable patients with suspected PE. MDCT-based angiography with more than 4 detector rows is superior to ventilation/perfusion nuclear scanning and is much faster than MRI (Schoepf and Costello 2004). Hence MDCT pulmonary angiography is the first line imaging modality for suspected PE patients. Its accuracy compared to the standard of reference invasive pulmonary angiography is congruent for ruling out PE. To achieve this standard in clinical practice CT imaging equipment with at least 16 detector row technology should be used (Figure 26-19). For latest CT technology the detection rate of subsegmental emboli

is even better than for invasive pulmonary angiography. MRI could potentially achieve the same results but for the majority of patients examination and acquisition time are too long.

Direct signs of pulmonary embolism on CT scans are intraluminal filling defects and lack of enhancement of a pulmonary artery. Acute emboli are trapped either at the pulmonary artery bifurcations (riding emboli) or in peripheral arteries that are smaller than the embolus. Complete occlusion of a vessel by a fresh embolus is possible but residual perfusion with a partial occlusion is more common. The typical presentation is a central filling defect with a ring of contrast enhancement representing residual perfusion around it.

The typical chest or cardiac CT angiography protocol has to be modified for PE detection. The ROI for contrast bolus tracking that initiates the scan is placed in the right heart to initiate scanning earlier compared to aortic or coronary CTA.

The most common factors leading to either false positive or false negative results are:

- Breathing artifacts may occur even with latest cutting edge equipment with a total breath-hold duration for the scan of less than 4 s. Both false positive and false negative results may ensue if the reader is unaware of the artifact.
- Pulsation artifacts predominantly affect the lung parenchyma adjacent to the cardiac structures (namely lingual

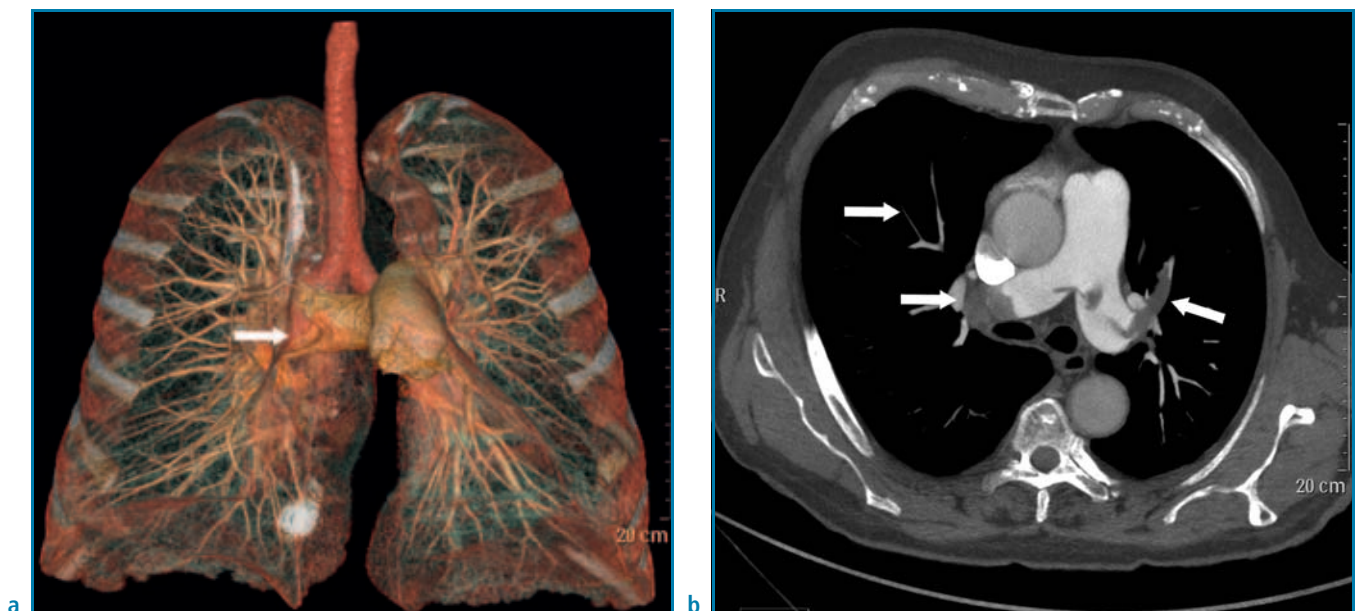


Figure 26-19 Pulmonary embolism: Volume rendering of the lungs with airways and pulmonary vasculature (a) shows a large filling defect (arrow) at the right main stem. A single axial slice from the volume stack (b) shows additional thrombi on the left side. The right

main stem appears completely amputated with total thrombus occlusion (arrow on left side of the image). The segmental artery supplying the lingula is filled with thrombus (right arrow).